A Novel Dynamic Membrane Reactor Concept with Radial-Flow Pattern for Reacting Material and Axial-Flow Pattern for Sweeping Gas in Catalytic Naphtha Reformers

Davood Iranshahi, Ehsan Pourazadi, Khadijeh Paymooni, and Mohammad Reza Rahimpour
School of Chemical and Petroleum Engineering, Dept. of Chemical Engineering,
Shiraz University, Shiraz 71345, Iran

DOI 10.1002/aic.12664
Published online May 23, 2011 in Wiley Online Library (wileyonlinelibrary.com).

Naphtha reforming units are of high interest for hydrogen production in refineries. In this regard, the application of membrane concept in radial-flow tubular naphtha reactors for hydrogen production is proposed. Because of the importance of the pressure drop problem in catalytic naphtha reforming units, the radial-flow reactors are proposed. A radial-flow tubular membrane reactor (RF-TMR) with the radial-flow pattern of the naphtha feed and the axial-flow pattern of the sweeping gas is proposed as an alternative configuration for conventional axial-flow tubular reactors (AF-TR). The cross-sectional area of the tubular reactor is divided into some subsections in which walls of the gaps between subsections are coated with the Pd-Ag membrane layer. A dynamic mathematical model considering radial and axial coordinates ((r, z)-coordinates) has been developed to investigate the performance of the new configuration. Results show ~300 and 11 kg/h increase in aromatic and hydrogen production rates in RF-TMR compared with AF-TR, respectively. Furthermore, smaller catalyst particles with higher efficiency can be used in RF-TMR due to a slight pressure drop. The enhancement in aromatics (octane number) and hydrogen productions owing to applying simultaneously the membrane concept and radial-flow pattern in naphtha reactors motivates the application of RF-TMR in refineries. © 2011 American Institute of Chemical Engineers *AIChE J,* 58: 1230–1247, 2012

Keywords: radial-flow naphtha reactor, hydrogen production, aromatic boosting, membrane separations, mathematical modeling

Introduction

Naphtha reforming

The catalytic reformer occupies a key position in a refinery, providing high value-added reformate for the gasoline pool; hydrogen for feedstock improvement by the hydrogen-consuming hydrotreatment processes; and frequently, benzene, toluene, and xylene aromatics for petrochemical uses. The hydrogen produced in catalytic reforming has become increasingly valuable as it is used in hydroprocessing units for removal of sulfur and nitrogen as well as for hydrocracking. The legislative requirements for sulfur removal from gasoline and diesel have increased hydrogen use in refineries; hence, refiners are looking for ways to maximize their hydrogen yields.[1] An extensive review of the catalytic naphtha reforming can be found throughout the literature. In most cases, researchers

Correspondence concerning this article should be addressed to M. R. Rahimpour at rahimpor@shirazu.ac.ir.

have tried to find proper catalyst functions by adding trace amount of some metals such as Sn, In, and Ge to improve the operation and selectivity of the catalyst and reduce the probability of coke formation on the catalyst surface. Studies are performed by Borgna et al.,[2] Boutzeloit et al.,[3] Viswanadham et al.,[4] Mazzieri et al.,[5] Dippolito et al.,[6] Pieck et al.,[7] Benitez et al.,[8,9] Le Peltier et al.,[10] and Carvalho et al.[11,12] in this regard. Furthermore, other researchers such as Weifeng et al.,[13] Ramage et al.,[14] Marin et al.,[15] Boyas and Froment,[16] Stijepovic et al.,[17] and Juarez and Macias[18] investigated detailed kinetic reactions to detect most of the components in the naphtha blend. Although such detailed kinetic reactions are beneficial, lumped paraffin, olefin, naphthene, and aromatic (PONA) kinetic reactions are enough for process engineers.[1] They are able to estimate the research octane number (RON) of the final product by considering the straight relationship between the RON and the weight fraction of aromatic groups in the reformate. Recently, Iranshahi et al. and Rahimpour et al. proposed new configurations including axial flow spherical naphtha reactor,[19] axial flow spherical membrane reactor,[20] radial flow spherical reactor,[21] isothermal reactor,[22] and thermally coupled fixed[23] and fluidized[24] bed heat exchanger reactors as alternative configurations for axial-flow tubular reactor (AF-TR) to boost hydrogen and aromatic production in refineries.

Hydrogen

Efficient, high performance and low cost technologies for producing hydrogen are urgently needed to encourage hydrogen utilization in the future. Hydrogen can be produced by several processes, including the steam reforming of methane and naphtha.[25] Refineries consume hydrogen in big amounts for removing sulfur and nitrogen compounds and producing lighter fuels. During the past decade, crude oil has been getting heavier and contains more sulfur and nitrogen, whereas the clean fuel specifications are progressively tightened along with the legislation for environmental protection. Consequently, more and more hydrotreating and hydrocracking processes are constructed, and hydrogen is now becoming a critical issue to the world's refiners.[26–28] Liao et al.[29] proposed a systematic approach for the retrofit design of hydrogen networks in refineries and tried to motivate the integrated management of hydrogen in the plant. Kumar et al.[30] determined the optimum distribution of hydrogen in the refinery using mathematical modeling. Other researches have been carried out on this subject in refineries and attempts have been made to optimize and minimize the use of hydrogen through the refinery complexes.[31,32]

Another remedy for the shortage of hydrogen in the refineries is to use membrane concept in the catalytic naphtha reactors to enhance the hydrogen production rate via shifting the dehydrogenation reaction toward the aromatic production.

Membrane reactor

Separation by membrane is less energy intensive, which requires no phase change in the process and typically provides low maintenance operation.[33] Membrane concept is a well-known technology for hydrogen purification and also one of the most cost effective and promising methods for high purity hydrogen production.[34] The Pd-Ag membrane layer with the silver content of 23–25% is extensively used for hydrogen separation.[35,36] Tosti et al.,[37] Shu et al.,[38] Koc et al.,[39] Wang et al.,[40] Mendes et al.,[41] Iulianelli et al.,[42] and Barbieri et al.[43] used Pd-based membranes for hydrogen production from steam reforming, dehydrogenation, and water-gas shift reactions. At the present time, membranes are used in refineries as many as 100 plants; hence, there exists a very large opportunity for increasing growth of membrane separation technology in future.[44] Recently, Rahimpour,[45] Mostafazadeh and Rahimpour,[46] and Rahimpour et al.[47] have proposed the application of hydrogen perm-selective membrane in the catalytic naphtha reactors to produce pure hydrogen as well as boosting the octane number.

In contrast to our previous publication,[47] this is a novel work which deals with the use of membrane concept in the radial flow tubular reactors (radial-flow tubular reactors are anticipated to be extensively licensed near future) instead of axial flow tubular reactors. A comparison is made between the top views of axial-flow tubular membrane reactor (AF-TMR)[47] and radial-flow tubular membrane reactor (RF-TMR) in Figure 1 to clarify the operation of these two configurations. As seen, the membrane in AF-TMR (Figure 1a) configuration is tubular end designed peripheral, whereas it is in a plate (sheet like) form and designed inside the reactor in RF-TMR (Figure 1b) configuration.

The underlying goal of this study is to investigate the performance of hydrogen perm-selective membrane assisted radial-flow naphtha reactors for hydrogen production and aromatic enhancement in naphtha reforming process. The sweeping gas composition changes along the axial direction (z-direction), whereas the fresh naphtha composition changes along the radial direction (r-direction). Set of PDEs are developed in this study, which is discussed later in the numerical solution section. Results demonstrate the superiority of this novel configuration to the conventional axial-flow tubular naphtha reactors. The developed mathematical model can be considered as an excellent tool for exploring the basic characteristics of such a novel configuration to achieve a primitive insight for future pilot plant design. Such explorations can contribute to considerable savings in money and time during the expensive stage of pilot plant development.

Process Description

Conventional naphtha reforming process (AF-TR)

Conventional systems use typically three or four axial flow tubular reactors with furnaces, which are assisted before each reactor. As the catalytic naphtha reforming process is highly endothermic, preheating is performed to compensate a reduction in the reaction rates. A recycle line is assisted in catalytic reformers, which recycles some of the produced hydrogen to the reactor and adjusts the H_2/HC in the reactors to reduce the possibility of coke formation in the reactor. More details and also a conceptual scheme of conventional catalytic naphtha reforming had been provided and discussed extensively in the previous work.[46]

Radial-flow tubular membrane reactor configuration

As pressure drop reduces the efficiency of AF-TR, RF-TMR is proposed as an alternative configuration because of

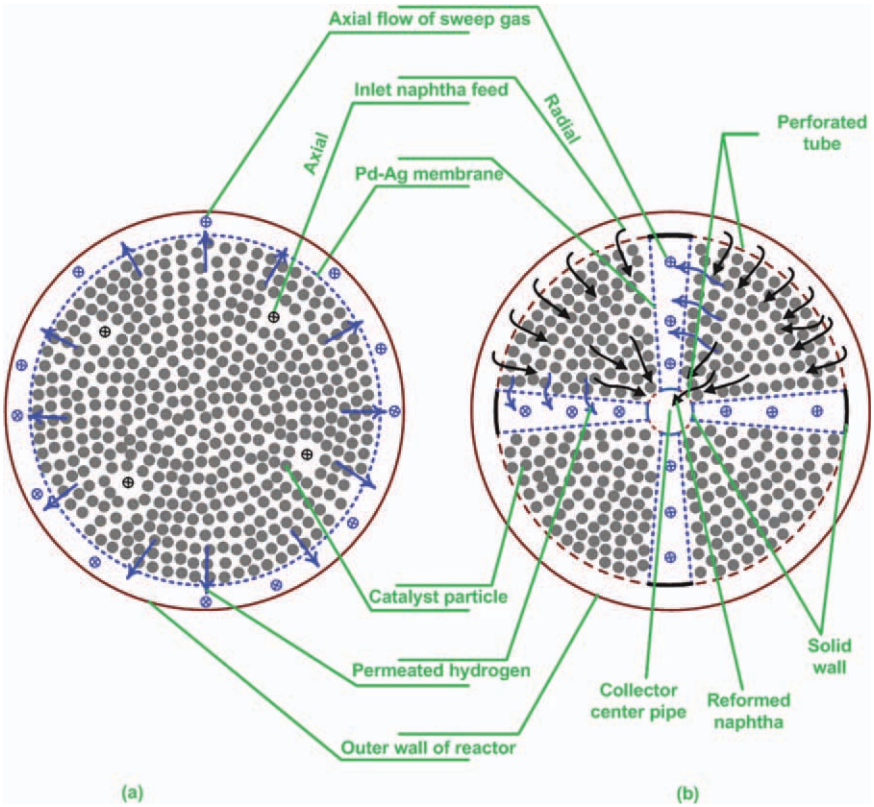

Figure 1. A comparison between the top views of AF-TMR (a) and RF-TMR (b) [note that the cross in circle symbol (⊗) represents the flow with downward direction (perpendicular to the page)].

[Color figure can be viewed in the online issue, which is available at wileyonlinelibrary.com.]

its slight pressure drop. A schematic diagram of RF-TMR plant for catalytic naphtha reforming process is shown in Figure 2a. As seen, the distribution lines of the sweeping gas are arranged in parallel. A comparison of RF-TMR and the AF-TR is shown in Figure 2b. Unlike AF-TR where the inlet naphtha feed is distributed uniformly along the axial direction, the inlet naphtha feed enters initially near the perforated wall of the outer annulus in RF-TMR then radially inward through the bed of catalytic particles. In RF-TMR, the naphtha feed flows radially through the packed bed, whereas the sweeping gas flows axially in the gaps (shell side). Attempts have been made to achieve a uniform flow distribution in the catalytic bed with the flow predominately in a radial direction. The chemical reactions take place on catalysts' surfaces. The internal design is such that flow enters the vessel across the entire cross section of the vessel, first proceeding downward near the wall of the vessel and then radially inward through the bed of catalytic particles and finally in a downward direction via an axial collector.[48] The reformed naphtha is collected by the axial collector. The flow patterns of the naphtha feed and the sweeping gas have been shown from the top view of RF-TMR in Figure 1. The radial-flow pattern of the naphtha feed through the catalytic bed is evidently illustrated in this figure. Also, the entrance of the sweeping gas along the reactor (in the axial coordinate) is obviously marked out in the shell side. Four subsections are considered in the cross-sectional area of the membrane reactor. The walls of the gaps between these subsections are coated by the Pd-Ag membrane layer, thus hydrogen permeates through the membrane layer and enters the shell side. The sweeping gas flows in the shell side and carries the permeated hydrogen. Table 1 reports some information and specification of the new configuration.

Reaction Scheme and Kinetic Expressions (Smith's Model)

As reaction kinetics play a paramount role in the performance of catalytic reforming model, attempts should be made to select a reliable kinetic expression. The naphtha used as catalytic reformer feedstock contains a mixture of more than 300 different chemical species including mainly paraffins, naphthenes, and aromatics in the carbon number range C_5–C_{12}. This overwhelming number of chemical components requires chemical component lumping into smaller set of kinetic lumps to make the reforming reactions network tractable.[1] To verify the feedstock or product qualities, it is often sufficient for the process engineers to know the PONA group concentrations.[1] Therefore, a kinetic model based on the Smith's model is taken into consideration in this study.[49] Smith considered naphtha feedstock to consist of three basic components and four dominant reactions as follows:

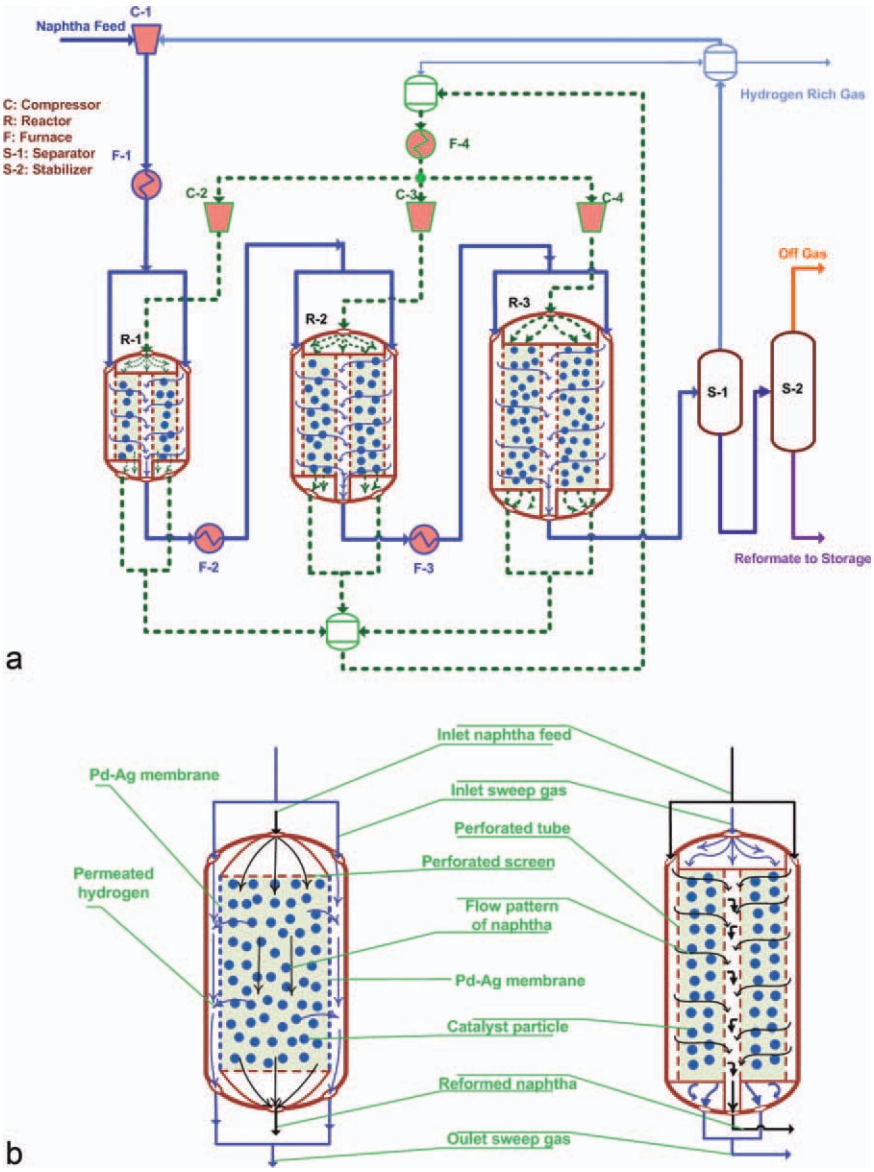

Figure 2. (a) A process flow diagram of membrane naphtha reforming unit and (b) a comparison of AF-TR and RF-TMR.

[Color figure can be viewed in the online issue, which is available at wileyonlinelibrary.com.]

- Dehydrogenation of naphthenes to aromatics

$$\text{Naphthenes } (C_nH_{2n}) \leftrightarrow \text{Aromatics } (C_nH_{2n-6}) + 3H_2 \quad (1)$$

- Dehydrocyclization of paraffins to naphthenes

$$\text{Naphthenes } (C_nH_{2n}) + H_2 \leftrightarrow \text{Paraffins } (C_nH_{2n+2}) \quad (2)$$

- Hydro cracking of naphthenes to lower hydrocarbons

$$\text{Naphthenes } (C_nH_{2n}) + n/3H_2 \rightarrow \text{Lighter ends } (C_1 - C_5) \quad (3)$$

- Hydro cracking of paraffins to lower hydrocarbons

$$\text{Paraffins } (C_nH_{2n+2}) + (n-3)/3H_2 \rightarrow \text{Lighter ends } (C_1 - C_5) \quad (4)$$

The rate equations of these reactions are expressed by:

$$r_1 = \left(\frac{k_{f1}}{K_{e1}}\right)(k_{e1}p_n - p_a p_h^3) \quad (5)$$

$$r_2 = \left(\frac{k_{f2}}{K_{e2}}\right)(k_{e2}p_n p_h - p_p) \quad (6)$$

$$r_3 = \left(\frac{k_{f3}}{p_t}\right)p_n \quad (7)$$

$$r_4 = \left(\frac{k_{f4}}{p_t}\right)p_p \quad (8)$$

Table 1. Specifications of Reactors, Feed, Product, and Catalyst of RF-TMR

Parameter	Numerical Value	Unit
Naphtha feed stock	30.41×10^3	kg/h
Reformate	24.66×10^3	kg/h
H_2/HC mole ratio	4.73	–
Liquid hourly space velocity	1.25	h^{-1}
Mole percent of hydrogen in recycle	69.5	–
Inner diameter, outer diameter, and length of 1st reactor	0.5, 1.54, 6.16	m
Inner diameter, outer diameter, and length of 2nd reactor	0.5, 1.75, 6.99	m
Inner diameter, outer diameter, and length of 3rd reactor	0.5, 2.05, 8.33	m
The number of sections for the1st reactor	4	–
The number of sections for the 2nd reactor	4	–
The number of sections for the 3rd reactor	4	–
Total membrane surface for the 1st reactor	25.63	m^2
Total membrane surface for the 2nd reactor	34.89	m^2
Total membrane surface for the 3rd reactor	51.15	m^2
The sweep pressure of 1st reactor	1545	kPa
The sweep pressure of 2nd reactor	2250	kPa
The sweep pressure of 3rd reactor	2348	kPa
Distillation fraction of naphtha feed and reformate		
True boiling point (K)	Naphtha feed (°C)	Reformate (°C)
Initial boiling pint (°C)	106	44
10%	113	73
30%	119	105
50%	125	123
70%	133	136
90%	144	153
Final boiling pint (°C)	173	181
Typical properties of catalyst		
d_p	1.2	mm
Pt	0.3	wt %
Re	0.3	wt %
S_a	220	m^2/g
ρ_b	0.3	kg/L
ε	0.36	–

The reaction rate constants ($\boldsymbol{k}_{f_i}$), equilibrium constants ($\boldsymbol{K}_{e_i}$), activation energies (E_i), and standard heat of reactions (ΔH_{298K}) are presented in Table 2.[50] The smith's model has been widely used due to its simplicity and accuracy.[1,51,52]

Mathematical Modeling

The following assumptions are made in the mathematical modeling of RF-TMR configuration:

- Homogeneous catalyst packed bed.
- Plug flow pattern is considered in the reactor.
- Axial diffusion of heat and mass are negligible compared with the convection.
- Reactions take place on the catalyst particles surface.
- Intrapellet heat and mass diffusion in catalyst pellet is neglected.
- Ideal gas law is applicable.
- Heat loss is neglected (outlet wall insulated).

Table 2. Rate Constants and Heat of Reactions for Naphtha Reforming

$k = A\exp(B - E/1.8T)$	A	B	E	ΔH_{198K}
k_{f_1}	9.87	23.21	36350	71038.06
k_{f_2}	9.87	35.98	58550	−36953.33
k_{f_3}	1	42.97	63800	−51939.31
k_{f_4}	1	42.97	63800	−56597.54
k_{e_1}	1.04×10^{-3}	46.15	46045	–
k_{e_2}	9.87	−7.12	8000	–

The below issues are supposed to be applied for the membrane layer:

- A supported membrane layer is used.
- Membrane is a hydrogen perm-selective layer.
- The Sievert's law is applicable.

In this work, attempts have been made to develop an accurate mathematical model for the membrane reactor. Therefore, a differential element as shown in Figure 3 is considered along the radial direction and the corresponding mass and energy balance equations in the radial and axial coordinates are developed. The corresponding mass and energy balance equations as well as the pressure drop correlation[53] and the catalyst deactivation model[54] are presented in Table 3. More explanation regarding this section is provided in Appendix.

Numerical Solution

The conceptual schemes for flow distribution in RF-TMR (a) and AF-TR (b) are clarified in Figures 4a, b. As the sweeping gas parameters such as temperature and composition change along the axial-coordinate, it influences indirectly on parameters of the reaction side. Therefore, the reactor length is divided into 500 segments, and the solution of each segment becomes the initial condition for the following one. Too many segments are considered along the axial-direction of RF-TMR to achieve more accurate results.

A two-step procedure is used to solve the set of partial differential-algebraic equations of the system. Set of coupled partial differential-algebraic equations have been solved by

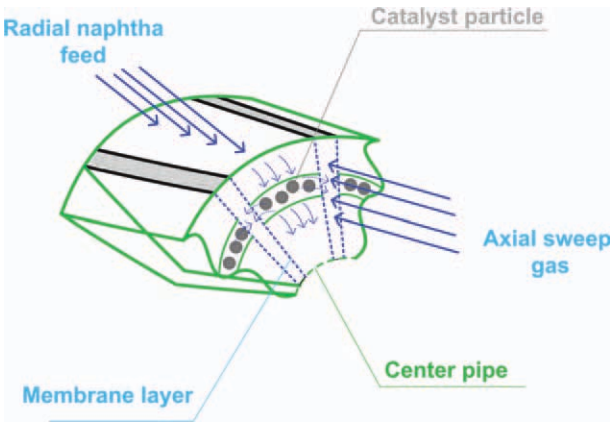

Figure 3. A differential element for mass and energy balances.

[Color figure can be viewed in the online issue, which is available at wileyonlinelibrary.com.]

Table 3. Mass and Energy Balances for RF-TMR

Fluid Phase (Reaction Side)

$$D_{ej}\frac{1}{A_{c_1}}\frac{\partial}{\partial r}\left(A_{c_1}\frac{\partial C_j}{\partial r}\right)-\frac{1}{A_{c_1}}\frac{\partial(u_{z_1}A_{c_1}C_j)}{\partial r}+\rho_b a\sum_{i=1}^{m}v_{ij}r_i-\begin{cases}\frac{P_{per}}{A_{c_1}}J_{H_2} & j=H_2\\ 0 & j\neq H_2\end{cases}=\varepsilon\frac{\partial C_j}{\partial t}\quad j=1,2,\ldots,n\ i=1,2,\ldots,m \tag{9}$$

$$C_T C_V \varepsilon\frac{\partial T}{\partial t}=RT\frac{\partial C_T}{\partial t}-u_r C_p\frac{\partial T}{\partial r}+\rho_b\sum_{i=1}r_i\Delta H_i+J_{H_2}\frac{\beta P_{per}}{A_{c_1}}(H^t_{H_2}-\gamma_{H_2})+\frac{P_{per}U}{A_{c_1}}(T^s-T) \tag{10}$$

$$\beta=U_{HVS}(P^t_{H_2}-P^s_{H_2})=\begin{cases}+1 & P^t_{H_2}\geq P^s_{H_2}\\ -1 & P^t_{H_2}<P^s_{H_2}\end{cases}\quad U_{HVS}\text{: Heaviside Function} \tag{11}$$

$$\gamma_{H_2}=(H^t_{H_2}-H^s_{H_2})U_{HVS}(P^t_{H_2}-P^s_{H_2})+H^s_{H_2}=\begin{cases}H^t_{H_2} & P^t_{H_2}\geq P^s_{H_2}\\ H^s_{H_2} & P^t_{H_2}<P^s_{H_2}\end{cases} \tag{12}$$

Fluid phase (sweep gas side)

$$D_{ej}\left(\frac{\partial^2 C_j}{\partial z^2}\right)-\frac{\partial(u_z C_j)}{\partial z}+\begin{cases}\frac{P_{per}}{A_{c_1}}J_{H_2} & j=H_2\\ 0 & j\neq H_2\end{cases}=\varepsilon\frac{\partial C_j}{\partial t}\quad j=1,2,\ldots,n\ i=1,2,\ldots,m \tag{13}$$

$$C_T C_V\varepsilon\frac{\partial T^s}{\partial t}=RT^s\frac{\partial C_T}{\partial t}+k_{eff}\left(\frac{\partial^2 T^s}{\partial z^2}\right)-u_z C_p\frac{\partial T^s}{\partial z}-J_{H_2}\frac{\beta P_{per}}{A_{c_2}}(H^t_{H_2}-\gamma_{H_2})-\frac{P_{per}U}{A_{c_2}}(T^s-T) \tag{14}$$

Hydrogen permeation rate

$$J_{H_2}=\frac{Q_0\exp(-\frac{E_{H_2}}{RT})}{\delta_{H_2}}\left(\sqrt{P^{tube}_{H_2}}-\sqrt{P^{shell}_{H_2}}\right)\quad Q_0=1.65\times10^{-5}\text{mol m}^{-1}\text{ s}^{-1}\text{ kPa}^{\frac{-1}{2}},E_{H_2}=15.7\text{ kJ mol}^{-1} \tag{15}$$

Additional relations

$$A_{c_1}=2\pi rL/\text{Number of subsections} \tag{16}$$

$$P_{per}=2L \tag{17}$$

Boundary and initial conditions

$$r=R_o: C_j=C_{j0}, T=T_0 \tag{18}$$

$$r=R_i: \frac{\partial C_j}{\partial r}=0, \frac{\partial T}{\partial r}=0 \tag{19}$$

$$z=0: C_j=C_{j0}, T=T_0 \tag{20}$$

$$z=L: \frac{\partial C_j}{\partial z}=0, \frac{\partial T}{\partial z}=0 \tag{21}$$

$$t=0; C_j=C^{ss}_j, T=T^{ss}, T_s=T^{ss}_s; a=1; \tag{22}$$

Ergun equation (pressure drop)

$$\frac{dP}{dr}=-\frac{G(1-\varepsilon)}{\rho g_c\phi_s d_p\varepsilon^3}\left(\frac{150(1-\varepsilon)\mu}{\phi_s d_p}+1.75G\right)\quad G\text{: mass flux kg/m}^2=\frac{\dot{m}}{A_{c_1}} \tag{23}$$

Catalyst deactivation

$$\frac{da}{dt}=-K_d\exp(-\tfrac{E_d}{R}(\tfrac{1}{T}-\tfrac{1}{T_R}))a^7\qquad T_R=770\text{ K},E_d=1.642\times10^5\text{J mol}^{-1},K_d=5.926\times10^{-5}\text{h}^{-1} \tag{24}$$

the orthogonal collocation method.[21] The procedure consists of a steady-state simulation before a dynamic simulation to obtain the initial conditions of the states along the reactor. Steady-state simulation of the reactor is performed by setting all time variations equal to zero and also by considering fresh catalysts with an activity of unity. Therefore, the results of the steady-state step are used as the initial conditions for the time-integration of the dynamic state equations in each node through the reactor.

The procedure of numerical solution is precisely explained for aromatic components in the first and the second reactors as follows.

The aromatic molar flow rate for both AF-TR and RF-TMR are presented in Table 4. The initial molar flow rate of aromatic fed to the first reactor is 39.21 kmol/h. This must be distributed over the surface area of reactor as shown in Figure 4a. In the modeling procedure, as shown in Figure 4c, the reactor is divided into 500 segments. The inlet aromatic molar flow rate for each segment is 39.21/500 kmol/h in the first reactor, and the total produced aromatic is 54.55 kmol/h in the first reactor. Thus, the outlet aromatic molar flow rate from each segment is (39.21 + 54.55)/500 kmol/h. The flow direction in each segment is radial and the outlet stream from each segment navigates to collector which has an axial flow and it is summed with the outlet of next segments. The aromatic molar flow rate is zero at beginning of collector pipe ($z = 0$ in Figure 4a). The same approach can be considered for the second reactor as shown in Figure 4d. The outlet aromatic molar flow rate from the first reactor is 93.76 kmol/h and introduces to the second reactor. The total produced aromatic in the second reactor is 29.44 kmol/h, and the produced aromatic in each segment is 29.44/500 kmol/h. Therefore, the outlet aromatic in each segment is (93.76 + 29.44)/500 kmol/h.

Model Validation

Steady-state model validation

To verify the efficiency of model under the steady-state condition, the model results are compared with observed plant data of AF-TR. Table 5 shows the plant data and the predicted mole fractions of components in the output of the system. Model results show a good agreement with the plant

Table 4. The Aromatic Molar Flow Rate for Both AF-TR and RF-TMR (kmol/h)

	First Reactor		Second Reactor		Third Reactor	
	Inlet	Outlet	Inlet	Outlet	Inlet	Outlet
AF-TR	39.21	92.68	92.68	121.8	121.8	133.4
RF-TMR	39.21	93.76	93.76	123.2	123.2	136.3

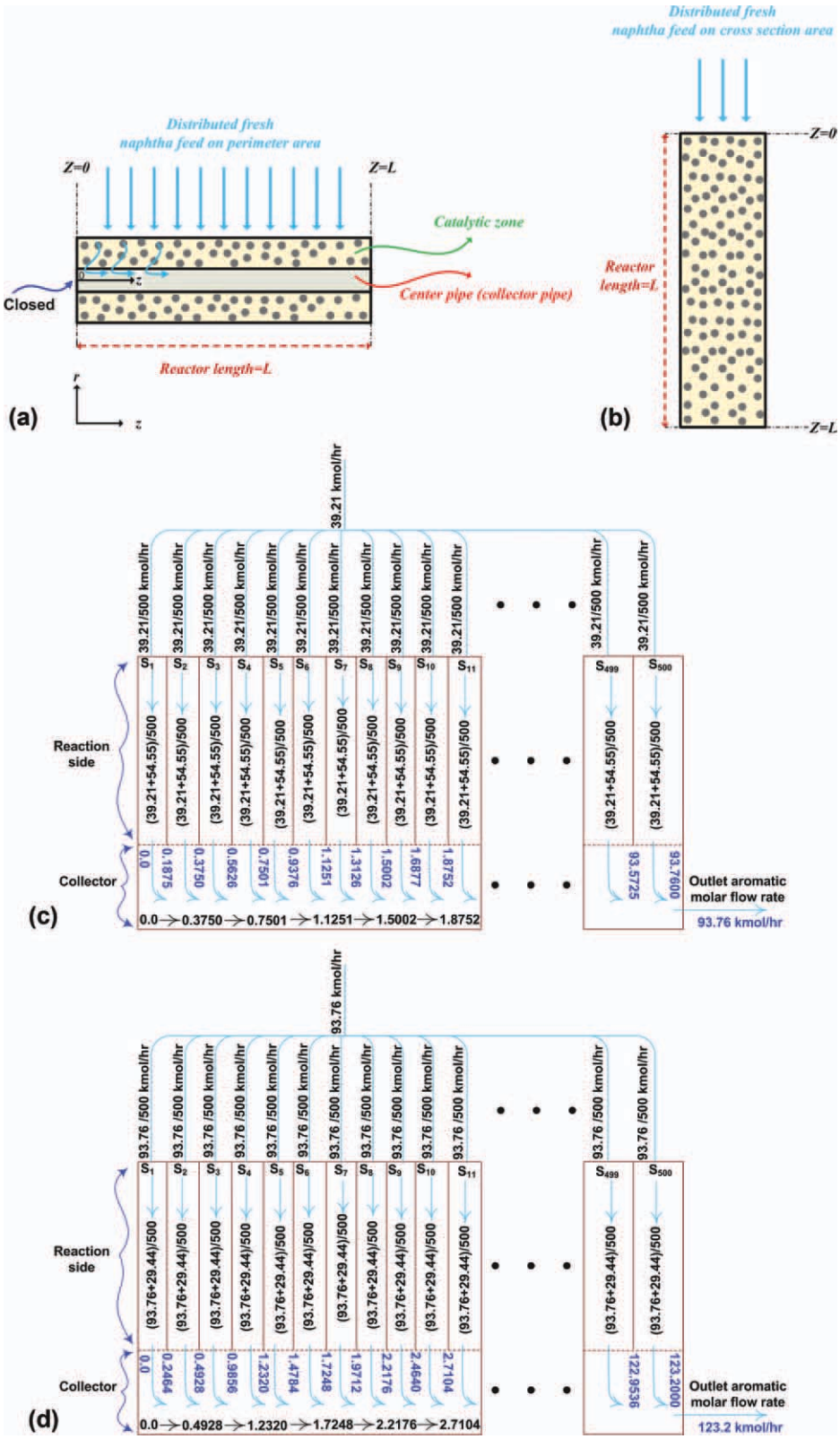

Figure 4. Feed distribution in the (a) RF-TMR, (b) AF-TR and a simplified schematic for numerical solution in the (c) first reactor and (d) the second reactor.

[Color figure can be viewed in the online issue, which is available at wileyonlinelibrary.com.]

Table 5. Comparison Between Model Prediction and Plant Data for Fresh Catalyst

Reactor No.	Inlet Temperature (K)	Inlet Pressure (kPa)	Catalyst Distribution (wt %)	Input Feedstock (mol %)	
1	777	3703	20	Paraffin	49.3
2	777	3537	30	Naphthene	36.0
3	775	3401	50	Aromatic	14.7

	Outlet Temperature (K)			Aromatic in Reformate (mol %)		
No.	Plant	AF-TR	RF-TMR	Plant	AF-TR	RF-TMR
1	722	727.30	732.85	–	34.67	35.56
2	753	750.98	756.55	–	47.19	48.13
3	770	770.53	772.35	57.70	56.18	58.35

data. Analyses of components (paraffin, naphthene, and aromatics) are performed by PONA test.[55] The PONA test is a GC apparatus, which operates with Helium as a carrier gas. The system is composed of three parts including split injector, temperature programmed oven, and the ionization detector. To detect all the individual compounds, more complex temperature program and also time are required. This test is usually taken monthly based on our data sheets from the domestic refinery.[1,55]

Unsteady state model validation

Model validation is also carried out by a comparison between the modeling results of AF-TR and the historical process data. The predicted results of production rate, the corresponding observed data, and the residual errors are presented in Table 6. As seen, the model performs well under industrial conditions and there exists a satisfactory well agreement between the daily-observed plant data and the modeling results.[55] The reported data for the plant are based on average daily values.

Results and Discussion

The results of the mathematical modeling of RF-TMR are illustrated in the following figures. The dimensionless reactor length and the dimensionless mass of catalyst represent the axial and the radial coordinates, respectively. In fact, the variation of parameters is investigated along the collector pipe of RF-TMR when the dimensionless length is discussed. However, the variation of parameters is investigated along the catalytic bed in the radial-direction when the dimensionless mass of catalyst is identified. At the beginning, the variation of parameters is investigated along the dimensionless reactor length (z-coordinate), afterward it is investigated along the dimensionless mass of catalyst (r-coordinate) in RF-TMR.

Variation of parameters along the dimensionless reactor length (z-coordinate)

The aromatic molar flow rate vs. the dimensionless lengths of AF-TR and RF-TMR is depicted in Figure 5a. The value of the aromatic molar flow rate is zero at the entrance of each reactor in RF-TMR configuration ($z = 0$, $z = 0.3$, and $z = 0.65$ related to the inlet of the collector pipe in the first, the second, and the third reactors, respectively), and it increases as proceeding along the axial-coordinate. In fact, the fresh naphtha feed is distributed over the surface area of the reactor (see Figure 4a) and undergoes the reactions as proceeding along the radius. Thus, the reaction medium is a short distance of reactor radius. Equations 18 and 19 imply that the corresponding equations are solved along the radial axis and the final products are gathered in the center pipe, which is actually a collecting container. Accordingly, the concentration of products and even the feed components start from zero when they are plotted along the collector pipe (axial direction). In a nutshell, the governing equations are solved by considering the boundary conditions along the radial direction; however, the flow rates are plotted here along the z-coordinate (collector pipe). The aromatic molar flow rate in each node (along the center pipe) is added to the following one to show the related molar flow rate. The sweeping gas flows axially in the permeation side of RF-TMR and provides a heating medium for the reaction side of each reactor. Thus, heat transfers from the shell side to the reaction side and increases the reaction rates. On the other hand, the dehydrogenation of naphthene to aromatics (Eq. 1) is the predominant reaction in naphtha reforming process; thus, the *in situ* hydrogen removal shifts this equilibrium reaction to the products side (according to the Le Chatelier's principle), which enhances the aromatic production rate. These factors boost the aromatic production rate in RF-TMR in comparison with AF-TR. The aromatic production rate increases by nearly 300 kg/h in RF-TMR.

The total hydrogen molar flow rate vs. the dimensionless reactor length is illustrated in Figure 5b. A proportion of the produced hydrogen in the first reactor permeats through the Pd-Ag membrane layer to the permeation side and it is carried by the sweeping gas to the second reactor. Afterward, this value is added to the produced hydrogen along the collector pipe (the axial coordinate) in the second reactor, and consequently, the value of the hydrogen molar flow rate in the second reactor does not start from zero at the inlet of the collector pipe ($z = 0.3$). The *in situ* hydrogen removal that shifts the first reaction (Eq. 1) to the products side and the sweeping gas in the shell side, which provides the required heat for highly endothermic naphtha reactions enhance the hydrogen production rate in RF-TMR compared with AF-TR.

In fact, refineries are focused mainly on improving and enhancing the aromatic production rate because the aromatic

Table 6. Unsteady State Model Validation

Time (day)	Inlet Temperature to the First Reactor (K)	Naphtha Feed (ton/h)	Plant (kmol/h)	AF-TR Model (kmol/h)	Devi % $\left(\frac{\text{Model}-\text{Plant}}{\text{Plant}}\right)\times 100$	RF-TMR (kmol/h)
0	777.0	30.41	225.90	221.78	−1.82	218.68
34	777.3	30.41	224.25	222.71	−0.68	219.67
62	777.8	31.00	229.65	228.13	−0.65	225.17
97	778.0	30.78	229.65	226.97	−1.16	224.06
125	778.5	31.22	229.65	231.00	0.59	228.14
160	778.7	31.22	229.65	231.48	0.79	228.66
188	777.2	28.55	211.60	210.02	−0.74	207.10
223	778.6	30.33	222.75	224.92	0.97	222.11
243	779.3	31.22	233.05	232.39	−0.28	229.64
298	779.2	30.67	228.65	228.38	−0.11	225.65
321	779.3	30.76	227.64	229.29	0.72	226.59
398	786.9	42.35	317.30	324.84	2.37	322.73
425	787.0	42.32	317.94	324.77	2.14	322.68
461	787.3	42.32	317.94	324.98	2.21	322.92
490	787.5	42.32	317.94	325.15	2.26	323.10
524	787.7	42.32	313.09	325.33	3.91	323.30
567	787.0	42.54	317.94	327.34	2.95	325.36
610	787.2	42.54	313.90	327.54	4.34	325.58
717	785.8	37.86	286.15	289.63	1.21	287.48
771	786.5	38.51	282.10	295.16	4.63	293.07

compounds have always an octane number (RON) above 100, and even small variations in aromatic and RON values influence significantly the production economics and engine performance.[1] Although the difference between the operation of AF-TR and RF-TMR seems to be marginal, it should be mentioned that the production rates have been plotted hourly. Figure 6 shows the superiority of RF-TMR to AF-TR regarding hydrogen and aromatic production.

Paraffin and naphthene are the most abundant hydrocarbons in petrochemical feedstock. In a typical straight-run naphtha, their concentrations vary between 40–70 wt % and 20–50 wt %, respectively. Naphthene plays a significant role in the reforming process because an increase in the octane number of the reformate can best be obtained by transformation of naphthene to aromatics.[1] Figure 7a illustrates the naphthene molar flow rate along AF-TR and RF-TMR. As previously mentioned, the naphthene molar flow rate is zero at the entrance of each reactor ($z = 0$, $z = 0.3$, and $z = 0.65$) (i.e., at the inlet of each collector pipe in three reactors). Although the naphthene molar flow rate decreases along the radial-coordinate through the reactor because of its consumption as a reactant, it increases as proceeding along the collector pipe in the axial-coordinate. In other words, the unreacted naphthenes in one node along the center pipe are added to the amount of the next node. Thus, the naphthene molar flow rate increases along the axial coordinate in the collector pipe. On the other hand, the slope of the solid lines decreases as proceeding from the first reactor to the third one because of less unreacted naphtha, which enters the subsequent reactor or further naphthene consumption as undergoes reaction in the subsequent reactors. The small graph illustrates that the naphthene consumption rate in RF-TMR is higher than the one in AF-TR because of its lower final molar flow rate.

The same trend is observed for the paraffin molar flow rate in Figure 7b. The paraffin consumption rate in RF-TMR increases 6.5 kmol/h in comparison with the one in

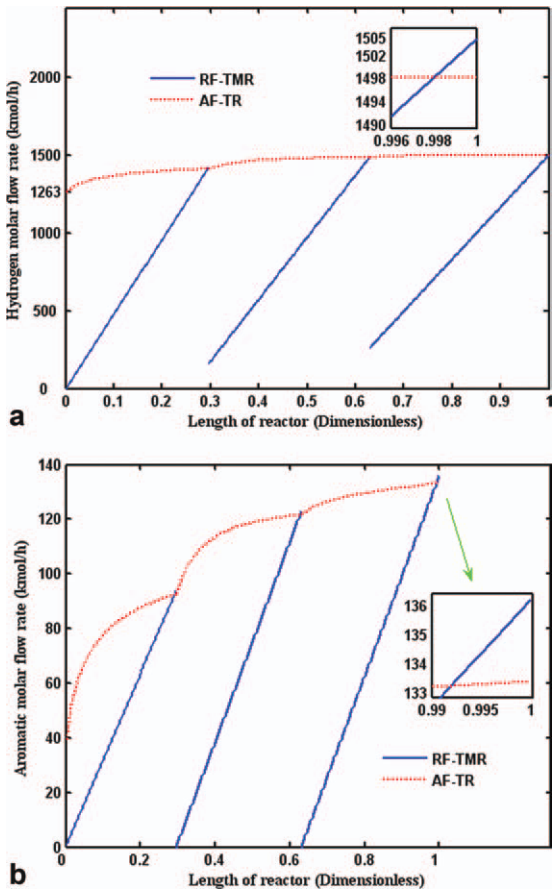

Figure 5. (a) Aromatic and (b) hydrogen molar flow rates vs. the axial direction in the collector (center pipe).

[Color figure can be viewed in the online issue, which is available at wileyonlinelibrary.com.]

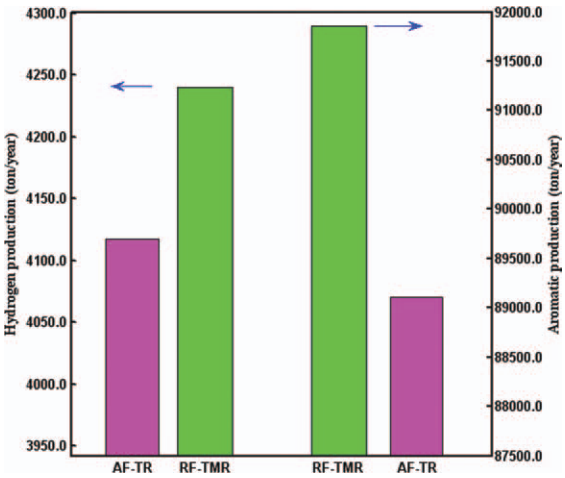

Figure 6. The annual hydrogen and aromatic production rates for AF-TR and RF-TMR.

[Color figure can be viewed in the online issue, which is available at wileyonlinelibrary.com.]

AF-TR. The same graph is depicted for the light ends molar flow rate in Figure 7c. As seen, the light ends production rate in RF-TMR is higher than the one in AF-TR. Light ends are used as a valuable feedstock for LPG in refineries.

Figure 8a expresses the temperature profile of the sweeping gas along RF-TMR. The inlet temperature of the sweeping gas to each reactor is 777 K owing to arranging a parallel configuration for the sweeping gas lines. As the endothermic dehydrogenation reaction of naphthenes to aromatics (Eq. 1) predominantly takes place in the reaction side of the first reactor, meanwhile, the temperature of the permeation side is proportional to the reaction side temperature, and the temperature drop in the first reactor is the highest. The hydrogen mole fraction in the sweeping gas along RF-TMR is demonstrated in Figure 8b. The hydrogen mole fraction in the sweeping gas increases along the reactors in RF-TMR owing to the hydrogen permeation through the Pd-Ag membrane layer to the shell side. The average hydrogen mole fraction in the outlet sweeping gas stream from the bottom of the container is about 78%.

The aromatic yield along the axial-coordinate of RF-TMR is shown in Figure 9. The aromatic yield is defined as net of aromatic production per unit mole of fresh naphtha feedstock as follows:

$$\text{Aromatic yield} = \frac{\Delta F_{\text{Aromatic}}}{F_{\text{Fresh naphtha feed}}}$$

The majority of naphthenes turn into aromatics in the first reactor. The percentage conversions of reactants and the aromatic yield are proportional to the sweeping gas temperature. They decrease as proceeding along the axial-coordinate of RF-TMR because of the decrease in the sweeping gas temperature along the reactor (see Figures 8a and 9). A majority of paraffins turn into light ends in third reactor mainly due to high temperature profile. In fact, the light ends production rate is accelerated by increasing the temperature (irreversible reactions 3 and 4). The decreasing trend of the aromatics yield in the first reactor is more considerable than the one in the other reactors due to the predominant reactions of aromatic production in the first reactor (a high temperature drop in the permeation side of the first reactor).

The 3-D plot of H_2/HC molar ratio vs. the radial and the axial coordinates of RF-TMR is depicted in Figure 10a. This

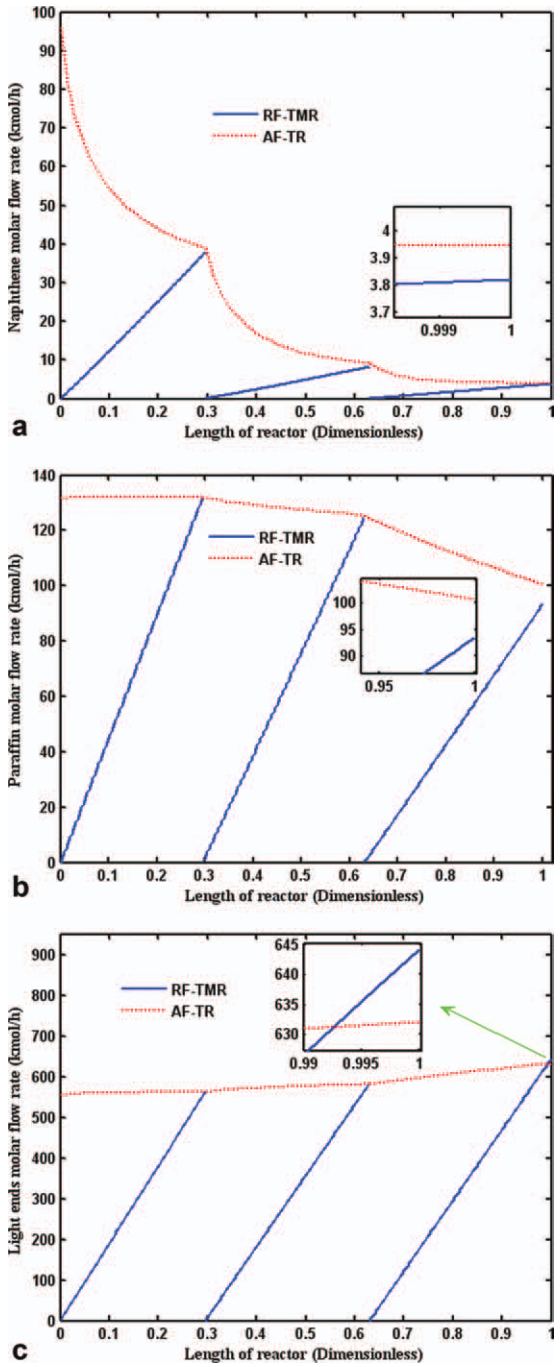

Figure 7. (a) Naphthene, (b) paraffin, and (c) light end molar flow rates along the axial coordinate in the RF-TMR and AF-TR.

[Color figure can be viewed in the online issue, which is available at wileyonlinelibrary.com.]

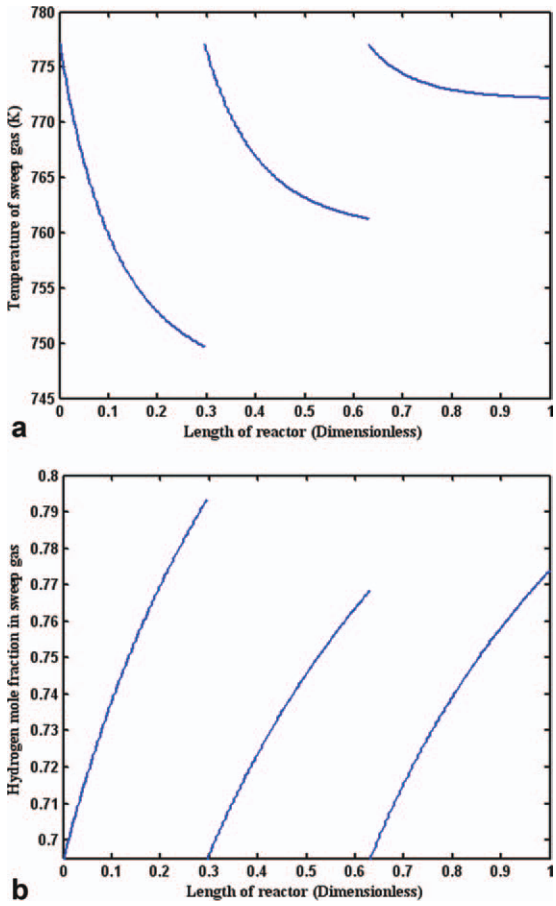

Figure 8. (a) Sweeping gas temperature profile and (b) hydrogen molar flow rate in the permeation side of the RF-TMR.

[Color figure can be viewed in the online issue, which is available at wileyonlinelibrary.com.]

ratio is one of the key parameters in the controlling unit of the naphtha reforming process. It is adjusted according to the amount of inlet fresh naphtha feed to the first reactor. If H_2/HC molar ratio becomes lower than 4,[55] the catalysts will be subjected to coking and a rapid deactivation. It imposes a huge burden on catalysts and jeopardizes the catalyst life. On the other hand, high ratios have undesired effects on the process conversion. In RF-TMR, the membrane layer maintains the H_2/HC molar ratio at approximately the inlet amount (4.73) by the help of the permeation pressures. The sweeping gas pressures for the first, the second, and the third reactors of RF-TMR are adjusted at 1545 kPa, 2250 kPa, and 2348 kPa, respectively. The related operating cost due to these high pressures can be reduced by increasing the hydrogen concentration in the sweeping gas. Hydrogen is produced as the reactants proceed along the reactor radius (radial-coordinate); therefore, the produced hydrogen is separated from the reaction side via the membrane layer. The difference between permeation and production rates here provides maxima in the radial coordinate of the RF-TMR profile. As far as the sweeping gas flows from $z = 0$ to $z = 1$, it becomes hydrogen rich and the driving force for the hydrogen permeation reduces. Indeed, the H_2/HC molar ratio of the reaction side increases slightly in the axial coordinate owing to an increase in the hydrogen content of the sweeping gas (lower permeation rate of hydrogen) at the end of RF-TMR ($z = 1$).

The naphthene and paraffin conversions are depicted in Figures 10b, c. The corresponding definition for conversion is as follows:

$$\text{Conversion} = \frac{\text{Input molar flow rate} - \text{Output molar flow rate}}{\text{Input molar flow rate}}$$

The naphthene conversion vs. the radial and the axial coordinates of RF-TMR are shown in Figure 10b. As seen, it increases remarkably along the radial-direction of RF-TMR unlike the axial-direction where its variation is not so considerable. The percentage of naphthene conversion decreases slightly as proceeding along the axial-direction because of a decrease in the sweeping gas temperature along the reactor.

Figure 10c illustrates the 3-D plot of the percentage conversion of paraffin. The paraffin molar flow rate increases slightly along the first reactor. Accordingly, based on the above description for the conversion, it is slightly negative in the first reactor (Output molar flow rate $\succ$ Input molar flow rate). The percentage conversion of paraffin reduces slightly along the axial-coordinate similar to the naphthene one due to temperature depletion in the permeation side. As the main reactions in the third reactor are cracking and dehydrocyclization (i.e., Eq. 4), the most paraffins turn into light ends in the third reactor.

Variation of parameters along the radial-coordinate of RF-TMR

In this section, the variation of parameters is investigated along the dimensionless mass of catalyst (r-coordinate). The percentage of paraffin conversion for AF-TR and RF-TMR (at the beginning and the end of the reactor in the axial-axis) is depicted in Figure 11a. The paraffin consumption rate in RF-TMR is higher than the one in AF-TR. However, in RF-TMR, the paraffin consumption rate at the beginning of the reactor ($z = 0$) is higher than the one at the end of the

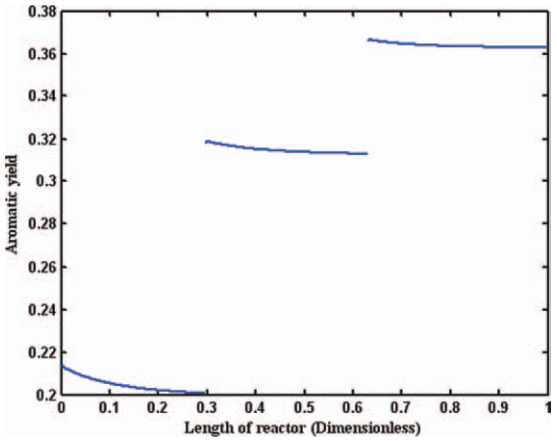

Figure 9. The aromatic yield in the axial coordinate of RF-TMR.

[Color figure can be viewed in the online issue, which is available at wileyonlinelibrary.com.]

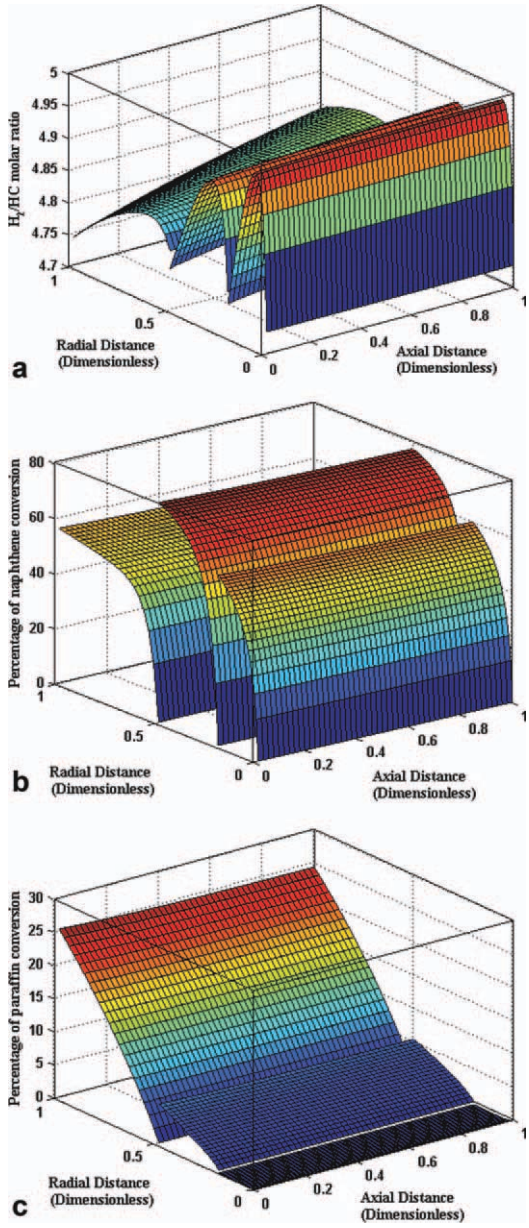

Figure 10. (a) H_2/HC molar ratio, (b) percentage conversion of naphthene, and (c) percentage conversion of paraffin vs. the dimensionless length and mass of catalyst.

[Color figure can be viewed in the online issue, which is available at wileyonlinelibrary.com.]

reactor ($z = 1$) because of a decrease in the sweeping gas temperature along the axial direction of the reactor. A discontinuity is observed in the paraffin consumption rate in RF-TMR because the average value of the paraffin consumption rate (between the inlet, $z = 0$, and the outlet, $z = 1$, values), which enters the following reactor is higher than the value at the outlet of the previous reactor (because the paraffin conversion decreases along the axial-coordinate).

Figure 11b shows the pressure profile vs. the dimensionless mass of catalysts of RF-TMR and AF-TR configurations. A negligible pressure drop is observed in RF-TMR, which allows the use of smaller catalyst particles with higher efficiency.

The temperature profile of the reaction side along the radial-coordinate (dimensionless mass of catalyst) of RF-TMR (at the beginning and the end of the reactor in the axial-

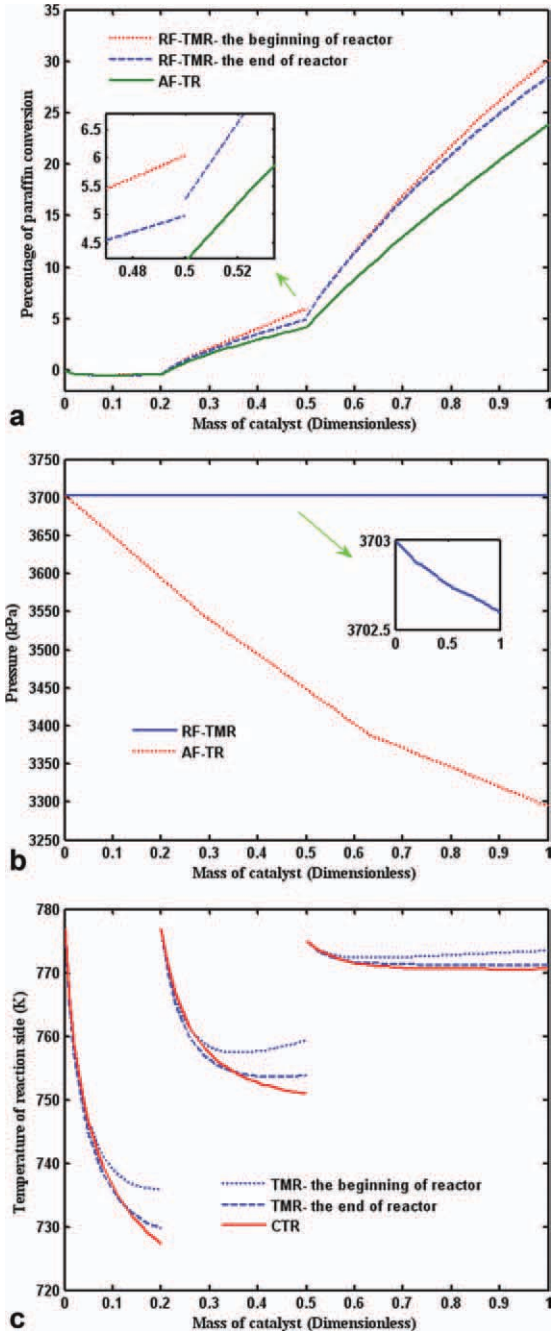

Figure 11. (a) Percentage conversion of paraffin, (b) pressure profile, and (c) the temperature profile in the reaction medium along the radial direction (dimensionless mass of catalyst).

[Color figure can be viewed in the online issue, which is available at wileyonlinelibrary.com.]

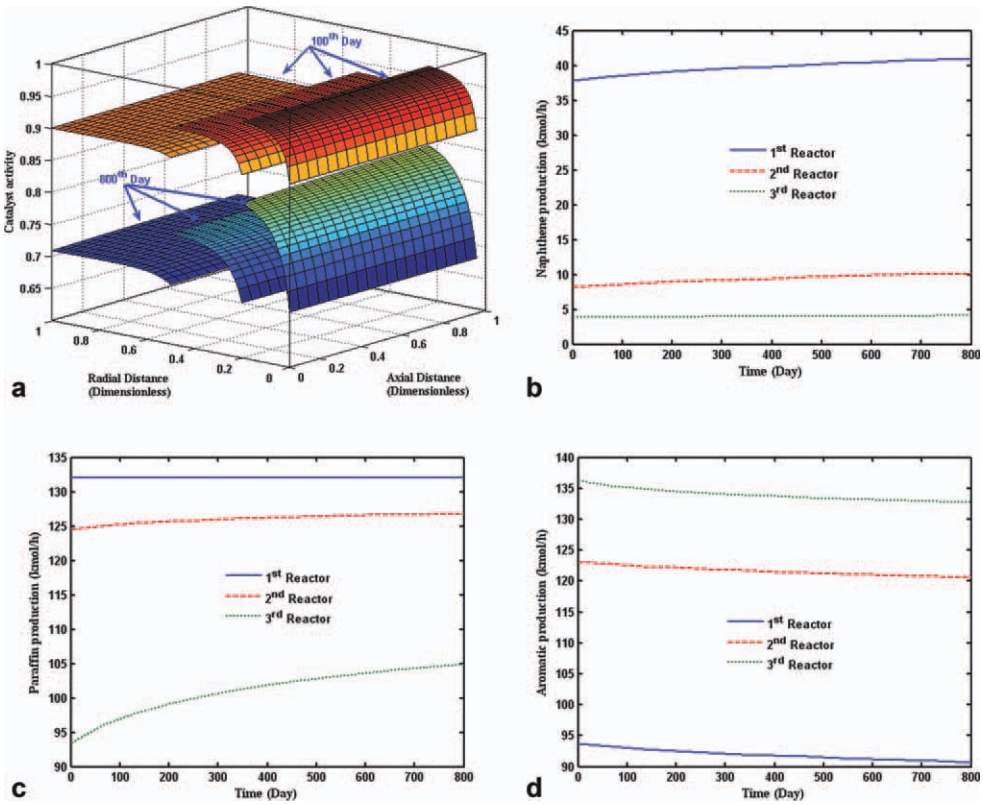

Figure 12. (a) Catalyst activity for 100th and 800th days of operation, (b) the naphthene, (c) the paraffin, and (d) the aromatic production for 800 days of operation.

[Color figure can be viewed in the online issue, which is available at wileyonlinelibrary.com.]

direction) and AF-TR is illustrated in Figure 11c. The reaction side temperature in RF-TMR is higher than the one in AF-TR. However, in RF-TMR, the temperature profile of the reaction side at the beginning of the reactor is higher than the one at the end of the reactor.

Time effect

Up to now, all the results have been investigated for the steady-state condition. The effect of time as an important parameter on RF-TMR performance is investigated through the following figures. The catalyst activity after 100th and 800th days of operation along RF-TMR is shown in Figure 12a. The catalyst activity has an inverse relationship with temperature based on Eq. 24. Consequently, higher catalyst activity can be achieved as proceeding along the reactor.

The naphthene and paraffin molar flow rates along each reactor vs. time is illustrated in Figures 12b, c. The amount of unreacted paraffin and naphthene increases with time, and however, aromatics production rate decreases with time because of catalyst deactivation (Figure 12d). Note that these figures have been plotted by considering the total inlet fresh naphtha feed equal to $30.41 \times 10^3 \frac{\text{kg}}{\text{h}}$ for all 800 days of operation just to show how the catalyst activity affects the production rates. In fact, the total fresh feed changes in the course of time due to the demands and downstream uses in refineries.

Conclusions

This study proposes the application of the membrane concept in the radial-flow naphtha reactors. A two-dimensional dynamic model considering radial and axial coordinates has been developed to investigate the effect of parameters along the dimensionless reactor length (z-coordinate) and mass of catalysts (r-coordinate). In this novel configuration, four subsections in the cross-sectional area of the membrane reactor have been taken into consideration. The modeling results of RF-TMR show a remarkable decrease in the pressure drop as well as an increase in the percentage conversion of reactants and products yield. The aromatic and hydrogen production rates increase considerably in this novel configuration about 265 kg per day and 7.2 ton per day, respectively. A comparison between the modeling results of RF-TMR and AF-TR demonstrates the superiority of the proposed configuration to AF-TR from the operational viewpoint. Because of the enhancement in aromatics and hydrogen production rates and an improvement in the reactor performance, RF-TMR is proposed as a promising configuration for naphtha reforming process in refineries. Another potential of the proposed configuration is that it can be used in the radial-flow moving bed reactors where the pack bed flows downward continuously. The optimization of the membrane thickness and some key parameters as well as the evaluation of the optimum number

of subsections can be proposed as a future work to have an entire judgment for future plant design.

Notation

a = catalyst activity
A_c = cross-sectional area, m^2
C = concentration, kmol m^{-3}
C_{j_0} = inlet concentration of component j, kmol m^{-3}
C_p = specific heat capacity at constant pressure, kJ $kmol^{-1}$ K^{-1}
C_T = total concentration, kmol m^{-3}
C_V = specific heat capacity at constant volume, kJ $kmol^{-1}$ K^{-1}
d_p = particle diameter, m
D_e = effective diffusivity, m^2 s^{-1}
E_d = activation energy of catalyst, J mol^{-1}
E_i = activation energy for ith reaction, kJ $kmol^{-1}$
F = molar flow rate, mol s^{-1}
k_{eff} = effective thermal conductivity, W m^{-1} s^{-1}
k_{c_i} = mass-transfer coefficient for component i, m h^{-1}
k_{f_1} = forward rate constant for reaction (1), kmol h^{-1} kg_{cat}^{-1} MPa^{-1}
k_{f_2} = forward rate constant for reaction (2), kmol h^{-1} kg_{cat}^{-1} MPa^{-2}
k_{f_3} = forward rate constant for reactions (3), kmol h^{-1} kg_{cat}^{-1}
k_{f_4} = forward rate constant for reactions (4), kmol h^{-1} kg_{cat}^{-1}
K_{e_1} = equilibrium constant, MPa^3
K_{e_2} = equilibrium constant, MPa^{-1}
K_d = deactivation constant of the catalyst, h^{-1}
L = length of reactor, m
m = number of reaction
M_i = molecular weight of component i, kg $kmol^{-1}$
n = number of component
N_i = molar flow rate of component i, kmol h^{-1}
P_i = partial pressure of ith component, kPa
P = total pressure, kPa
Q = volumetric flow rate, m^3 s^{-1}
r = radius, m
r_i = rate of reaction for ith reaction, kmol kg_{cat}^{-1} h^{-1}
R = gas constant, kJ $kmol^{-1}$ K^{-1}
S_a = specific surface area of catalyst pellet, m^2 kg^{-1}
t = time, h
T = temperature of gas phase, K
T_R = reference temperature, K
u_r = radial velocity, m s^{-1}
y_i = mole fraction for ith component in gas phase
z = variable represent length of reactor, m

Greek letters

Δ = net of production
ε = void fraction of catalyst bed
μ = viscosity of gas phase, kg m^{-1} s^{-1}
ρ = density of gas phase, kg m^{-3}
ρ_b = reactor bulk density, kg m^{-3}
σ = tensile stress, N m^{-2}
ϕ_s = sphericity

Subscript and superscripts

ΔH = heat of reaction, kJ $kmol^{-1}$ of H_2
A = aromatic
H_2 = hydrogen
i = numerator for reaction
j = numerator for component
N = naphthene
P = paraffin
s = sweep side
ss = steady state
t = tube side

Abbreviations

AF-TR = axial flow tubular reactor
AF-TMR = axial flow tubular membrane reactor
Pt = platinum
Re = rhenium
RF-TMR = radial flow tubular membrane reactor
RON = research octane number
WHSV = weight hourly space velocity, h^{-1}

Literature Cited

1. Antos GA, Aitani AM. *Catalytic Naphtha Reforming*, 2nd ed. New York: Marcel Dekker Inc., 1995.
2. Borgna A, Garetto TF, Apestegua CR, Moraweck B. Formation of bimetallic alloys in naphtha reforming Pt-Ge/Al2O3 catalysts: an EXAFS study. *Appl Catal A*. 1999;182:189–197.
3. Boutzeloit M, Benitez VM, Mazzieri VA, Especel C, Epron F, Vera CR, Pieck CL, Marecot P. Effect of the method of addition of Ge on the catalytic properties of Pt–Re/Al2O3 and Pt–Ir/Al2O3 naphtha reforming catalysts. *Catal Commun*. 2006;7:627–632.
4. Viswanadham N, Kamble R, Sharma A, Kumar M, Saxena AK. Effect of Re on product yields and deactivation patterns of naphtha reforming catalyst. *J Mol Catal A Chem*. 2008;282:74–79.
5. Mazzieri VA, Pieck CL, Vera CR, Yori JC, Grau JM. Effect of Ge content on the metal and acid properties of Pt-Re-Ge/Al2O3-Cl catalysts for naphtha reforming. *Appl Catal A*. 2009;353:93–100.
6. Dippolito SA, Vera CR, Epron F, Samoila P, Especel C, Marecot P, Gutierrez LB, Pieck CL. Influence of tin addition by redox reaction in different media on the catalytic properties of Pt-Re/Al2O3 naphtha reforming catalysts. *Appl Catal A*. 2009;370:34–41.
7. Pieck CL, Vera CR, Parera JM, Gime'nez GN, Serra LR, Carvalho LS, Rangel MC. Metal dispersion and catalytic activity of trimetallic Pt-Re-Sn/Al_2O_3 naphtha reforming catalysts. *Catal Today*. 2005; 107–108:637–642.
8. Benitez VM, Vera CR, Rangel MC, Yori JC, Grau JM, Pieck CL. Modification of multimetallic naphtha-reforming catalysts by indium addition. *Ind Eng Chem Res*. 2009;48:671–676.
9. Benitez V, Boutzeloit M, Mazzieri VA, Especel C, Epron F, Vera CR, Marécot P, Pieck CL. Preparation of trimetallic Pt–Re–Ge/Al_2O_3 and Pt–Ir–Ge/Al_2O_3 naphtha reforming catalysts by surface redox reaction. *Appl Catal A*. 2007;319:210–217.
10. Le Peltier F, Deves JM, Clause O, Kolenda F, Brunard N. *U.S. Patent* 6,511,593, 2003.
11. Carvalho LS, Pieck CL, Rangel MC, Fígoli NS, Grau JM, Reyesc P, Parera JM. Trimetallic naphtha reforming catalysts. I. Properties of the metal function and influence of the order of addition of the metal precursors on Pt–Re–Sn/Al_2O_3–Cl. *Appl Catal A*. 2004;269: 91–103.
12. Carvalho LS, Pieck CL, Rangel MC, Figoli NS, Vera CR, Parera JM. Trimetallic naphtha reforming catalysts. II. Properties of the acid function and influence of the order of addition of the metallic precursors on Pt-Re-Sn/-Al_2O_3-Cl. *Appl Catal A*. 2004;269:105–116.
13. Weifeng H, Hongye S, Yongyou H, Jian C. Lumped kinetics model and its on-line application to commercial catalytic naphtha reforming process. *J Chem Ind Eng*. 2006;57:1605–1611.
14. Ramage MP, Graziani KP, Krambeck FJ. 6 Development of Mobil's kinetic reforming model. *Chem Eng Sci*. 1980;35:41–48.
15. Marin GB, Froment GF, Lerou JJ, De Backer W. Simulation of a catalytic naphtha reforming unit W. *Eur Fed Chem Eng*. 1983;2: 1–7.
16. Boyas RS, Froment GF. Fundamental kinetic modeling of catalytic reformer. *Ind Eng Chem Res*. 2009;48:1107–1119.
17. Stijepovic MZ, Ostojic AV, Milenkovic I, Linke P. Development of a kinetic model for catalytic reforming of naphtha and parameter estimation using industrial plant data. *Energy Fuels*. 2009;23: 979–983.
18. Juarez JA, Macias EV. Kinetic modeling of naphtha catalytic reforming reactions. *Energy Fuels*. 2000;14:1032–1037.
19. Iranshahi D, Pourazadi E, Paymooni K, Bahmanpour AM, Rahimpour MR, Shariati A. Modeling of an axial flow, spherical packed-bed reactor for naphtha reforming process in the presence of the catalyst deactivation. *Int J Hydrogen Energy*.2010;35:12784–12799.
20. Rahimpour MR, Iranshahi D, Pourazadi E, Paymooni K, Bahmanpour AM. The aromatic enhancement in the axial-flow spherical packed-bed membrane naphtha reformers in the presence of catalyst deactivation. *AIChE J*. In press. DOI: 10.1002/aic.12529.

21. Iranshahi D, Rahimpour MR, Asgari A. A novel dynamic radial-flow, spherical-bed reactor concept for naphtha reforming in the presence of catalyst deactivation. *Int J Hydrogen Energy*. 2010;35: 6261–6275.
22. Iranshahi D, Pourazadi E, Paymooni K, Rahimpour MR. Enhancement of aromatic production in naphtha reforming process by simultaneous operation of isothermal and adiabatic reactors. *Int J Hydrogen Energy*. 2011;36:2076–2085.
23. Iranshahi D, Bahmanpour AM, Pourazadi E, Rahimpour MR. Mathematical modeling of a multi-stage naphtha reforming process using novel thermally coupled recuperative reactors to enhance aromatic production. *Int J Hydrogen Energy*. 2010;35:10984–10993.
24. Rahimpour MR, Vakili R, Pourazadi E, Iranshahi D, Paymooni K. A novel integrated, thermally coupled fluidized bed configuration for catalytic naphtha reforming to enhance aromatic and hydrogen productions in refineries. *Int J Hydrogen Energy*. 2011;36:2979–2991.
25. Onozaki M, Watanabe K, Hashimoto T, Saegusa H, Katayama Y. Hydrogen production by the partial oxidation and steam reforming of tar from hot coke oven gas. *Fuel*. 2006;85:143–149.
26. Alves JJ, Towler GP. Analysis of refinery hydrogen distribution systems. *Ind Eng Chem Res*. 2002;41:5759–5769.
27. Hallale N, Moore I, Vauk D. Hydrogen: liability or asset? *Chem Eng Prog*. 2002;98:66–75.
28. Liu F, Zhang N. Strategy of purifier selection and integration in hydrogen networks. *Chem Eng Res Des*. 2004;82:1315–1330.
29. Liao Z, Wang J, Yang Y, Rong G. Integrating purifiers in refinery hydrogen networks: a retrofit case study. *J Clean Prod*. 2010;18: 233–241.
30. Kumar A, Gautami G, Khanam S. Hydrogen distribution in the refinery using mathematical modeling. *Energy*. 2010;35:3763–3772.
31. Hallale N, Liu F. Refinery hydrogen management for clean fuels production. *Adv Environ Sci*. 2001;6:81–98.
32. Towler GP, Mann R, Serriere AJL, Gabaude CMD. Refinery hydrogen management: cost analysis of chemically-integrated facilities. *Ind Eng Chem Res*. 1996;35:2378–2388.
33. Rahimpour MR, Pourazadi E. A comparison of hydrogen and methanol production in a thermally coupled membrane reactor for co-current and counter-current flows. *Int J Energy Res*. In press. DOI: 10.1002/er.1744.
34. Yang JY, Nishimura C, Komaki M. Hydrogen permeation of $Pd_{60}Cu_{40}$ alloy covered V–15Ni composite membrane in mixed gases containing H_2S. *J Membr Sci*. 2008;309:246–250.
35. Nam SE, Lee KH. Hydrogen separation by Pd alloy composite membranes: introduction of diffusion barrier. *J Membr Sci*. 2001;192:177–185.
36. Okazaki J, Tanaka DAP, Tanco MAL, Wakui Y, Mizukami F, Suzuki TM. Hydrogen permeability study of the thin Pd–Ag alloy membranes in the temperature range across the α-β phase transition. *J Membr Sci*. 2006;282:370–374.
37. Tosti S, Basile A, Bettinali L, Borgognoni F, Gallucci F, Rizzello C. Design and process study of Pd membrane reactors. *Int J Hydrogen Energy*. 2008;33:5098–5105.
38. Shu J, Grandjean BPA, Neste AV, Kaliaguine S. Catalytic palladium-based membrane reactors: a review. *Can J Chem Eng*. 1991; 69:1036–1060.
39. Koc R, Kazantzis NK, Ma YH. A process dynamic modeling and control framework for performance assessment of Pd/alloy-based membrane reactors used in hydrogen production. *Int J Hydrogen Energy*. 2011;36:4934–4951.
40. Wang L, Murata K, Inaba M. Production of pure hydrogen and more valuable hydrocarbons from ethane on a novel highly active catalyst system with a Pd-based membrane reactor. *Catal Today*. 2003;82:99–104.
41. Mendes D, Chibante V, Zheng J, Tosti S, Borgognoni F, Mendes A, Madeira LM. Enhancing the production of hydrogen via water–gas shift reaction using Pd-based membrane reactors. *Int J Hydrogen Energy*. 2010;35:12596–12608.
42. Iulianelli A, Manzolini G, De Falco M, Campanari S, Longo T, Liguori S, Basile A. H_2 production by low pressure methane steam reforming in a Pd–Ag membrane reactor over a Ni-based catalyst: experimental and modeling. *Int J Hydrogen Energy*. 2010;35:11514–11524.
43. Barbieri G, Brunetti A, Tricoli G, Drioli E. An innovative configuration of a Pd-based membrane reactor for the production of pure hydrogen: experimental analysis of water gas shift. *J Power Sources*. 2008;182:160–167.
44. Baker RW. Future directions of membrane gas separation technology. *Ind Eng Chem Res*. 2002;41:1393–1411.
45. Rahimpour MR. Enhancement of hydrogen production in a novel fluidized-bed membrane reactor for naphtha reforming. *Int J Hydrogen Energy*. 2009;34:2235–2251.
46. Mostafazadeh AK, Rahimpour MR. A membrane catalytic bed concept for naphtha reforming in the presence of catalyst deactivation. *Chem Eng Process*. 2009;48:683–694.
47. Rahimpour MR, Iranshahi D, Pourazadi E, Bahmanpour AM. A comparative study on a novel combination of spherical and membrane tubular reactors of the catalytic naphtha reforming process. *Int J Hydrogen Energy*. 2011;36:505–517.
48. Bolton GT, Hooper CW, Mann R, Stitt EH. Flow distribution and velocity measurement in a radial flow fixed bed reactor using electrical resistance tomography. *Chem Eng Sci*. 2004;59:1989–1997.
49. Smith RB. Kinetic analysis of naphtha reforming with platinum catalyst. *Chem Eng Prog*. 1959;55:76–80.
50. Rase RF. *Chemical Reactor Design for Process Plants*, Vol. 2. New York: Wiley, 1977.
51. Liang KM, Guo HY, Pan SW. A study on naphtha catalytic reforming reactor simulation and analysis. *J Zhejiang Univ Sci*. 2005;6B:590–596.
52. Bommannan D, Srivastava RD, Saraf DN. Modeling of catalytic naphtha reformers. *Can J Chem Eng*. 1989;67:405–411.
53. Fogler HS. *Elements of Chemical Reaction Engineering*, 2nd ed. NJ: Prentice-Hall Englewood Cliffs, 1992.
54. Rahimpour MR, Esmaili S, Bagheri GNA. Kinetic and deactivation model for industrial catalytic naphtha reforming. Iran. *J Sci Technol Trans Sect B*. 2003;27:279–290.
55. Operating Data of Catalytic Reformer Unit, Domestic Refinery, 2005.
56. Barbieri G, Marigliano G, Golemme G, Drioli E. Simulation of CO_2 hydrogenation with CH3OH removal in a zeolite membrane reactor. *Chem Eng J*. 2002;85:53–59.

Appendix: Developing of Governing Equations

Mass balance

The derivation of governing equations (mass and energy balances) have been presented here.

Considering the Sievert's law, the absolute difference of square roots of partial pressure must be considered and the permeated hydrogen molar flux (J_{H_2}) is positive.

$$J_{H_2} = \frac{Q_0 \exp(-\frac{E_{H_2}}{RT})}{\delta_{H_2}} (|\sqrt{P_{H_2}} - \sqrt{P_{H_2}^{Shell}}|) \qquad (A1)$$

The mass balance for a control volume with length of dz and cross-sectional area of A_c is:

$$\text{Input} - \text{Output} + \text{Consumption} + \text{Permeation through the Membrane} = \text{Accumulation} \qquad (A2)$$

$$(N_j \times A_c)|_z - (N_j \times A_c)|_{z+dz} + a \times \rho_b \sum_{i=1}^{m} v_{ij} r_i \times A_c \times dz - P_{Per} \times dz \times \begin{cases} 0 & j \neq H_2 \\ J_{H_2} & j = H_2, P_{H_2}^t \geq P_{H_2}^s \\ -J_{H_2} & j = H_2, P_{H_2}^s \geq P_{H_2}^t \end{cases} = \frac{\partial n_j}{\partial t} \; j = 1,2,...,n \; i = 1,2,...,m \qquad (A3)$$

n_j is mole of component j in control volume. The Pd-Ag membrane is exclusively permeable for hydrogen and insulated for other components.

By writing the Taylor's extension of second term in left-hand side of the equation, one can obtain:

$$-\frac{\partial(N_j \times A_c)}{\partial z}.dz + a \times \rho_b \sum_{i=1}^{m} v_{ij} r_i \times A_c \times dz - P_{Per} \times dz \times \begin{cases} 0 & j \neq H_2 \\ J_{H_2} & j = H_2, P^t_{H_2} \geq P^s_{H_2} \\ -J_{H_2} & j = H_2, P^s_{H_2} \geq P^t_{H_2} \end{cases} = \frac{\partial n_j}{\partial t} \quad \text{(A4)}$$

Now the above equation is divided by the volume of the differential element:

$$-\frac{1}{A_c}\frac{\partial(N_j \times A_c)}{\partial z} + a \times \rho_b \sum_{i=1}^{m} v_{ij} r_i - \frac{P_{Per}}{A_c} \times \begin{cases} 0 & j \neq H_2 \\ J_{H_2} & j = H_2, P^t_{H_2} \geq P^s_{H_2} \\ -J_{H_2} & j = H_2, P^s_{H_2} \geq P^t_{H_2} \end{cases} = \frac{1}{A_c \times dz}\frac{\partial n_j}{\partial t} \quad \text{(A5)}$$

or

$$-\frac{\partial(N_j)}{\partial z} - \frac{N_j}{A_c}\frac{\partial(A_c)}{\partial z} + a \times \rho_b \sum_{i=1}^{m} v_{ij} r_i - \frac{P_{Per}}{A_c} \times \begin{cases} 0 & j \neq H_2 \\ J_{H_2} & j = H_2, P^t_{H_2} \geq P^s_{H_2} \\ -J_{H_2} & j = H_2, P^s_{H_2} \geq P^t_{H_2} \end{cases} = \frac{1}{A_c \times dz}\frac{\partial n_j}{\partial t} \quad \text{(A6)}$$

which N_j is molar flux of component j. The molar flux consists of two terms: the first term is due to bulk motion and the second term is diffusion of component j as follows:

$$N_j = -D_{ej}\frac{\partial C_j}{\partial z} + C_j u_Z \quad \text{(A7)}$$

Concentration of component j in control volume equals the mole of component j in volume of fluid. Whereas the volume of fluid is ε times of the volume of control volume element, one can obtain:

$$C_j = \frac{n_j}{(A_c \times dz \times \varepsilon)} \quad \text{(A8)}$$

or

$$n_j = C_j \times (A_c \times dz \times \varepsilon) \quad \text{(A9)}$$

by substituting the above equation in governing mass balance equation, we have:

$$D_{ej}\frac{1}{A_c}\frac{\partial}{\partial z}\left(A_c\frac{\partial C_j}{\partial z}\right) - \frac{1}{A_c}\frac{\partial}{\partial z}(A_c u_z C_j) + \rho_b a \sum_{i=1}^{m} v_{ij} r_i - \frac{P_{Per}}{A_c} \times \begin{cases} 0 & j \neq H_2 \\ J_{H_2} & j = H_2, P^t_{H_2} \geq P^s_{H_2} \\ -J_{H_2} & j = H_2, P^s_{H_2} \geq P^t_{H_2} \end{cases} = \varepsilon\frac{\partial C_j}{\partial t} \begin{matrix} j = 1,2,...,n \\ i = 1,2,...,m \end{matrix} \quad \text{(A10)}$$

Energy balance

By applying the first law of thermodynamic, the related energy balance is as follow:

$$\begin{pmatrix} \text{Rate of} \\ \text{accumulation} \\ \text{of energy} \\ \text{within the} \\ \text{system} \end{pmatrix} = \begin{pmatrix} \text{Rate of} \\ \text{energy added} \\ \text{to the system} \\ \text{by conduction} \\ \text{heat transfer} \end{pmatrix} + \begin{pmatrix} \text{Rate of} \\ \text{energy leaving} \\ \text{the system} \\ \text{by conduction} \\ \text{heat transfer} \end{pmatrix} + \begin{pmatrix} \text{Rate of} \\ \text{work done} \\ \text{by the} \\ \text{system on the} \\ \text{surroundings} \end{pmatrix} + \begin{pmatrix} \text{Rate of energy} \\ \text{added to the} \\ \text{system by mass} \\ \text{flow into the} \\ \text{system} \end{pmatrix} + \begin{pmatrix} \text{Rate of energy} \\ \text{leaving} \\ \text{system by mass} \\ \text{flow out of} \\ \text{the system} \end{pmatrix} + \begin{pmatrix} \text{Rate of} \\ \text{flow of heat} \\ \text{to the system} \\ \text{from the} \\ \text{surroundings} \end{pmatrix} + \begin{pmatrix} \text{Rate of energy added to} \\ \text{(leaving) the system by} \\ \text{permeated mass of} \\ \text{hydrogen flow into} \\ \text{(out of) the system} \end{pmatrix} \quad \text{(A11)}$$

Considering the reaction side as the system, the permeation side will be as the surrounding. The energy balance in the absence of shaft work is:

$$-K_{eff}A_c\frac{\partial T}{\partial z}\Big|_Z - K_{eff}A_c\frac{\partial T}{\partial z}\Big|_{Z+dZ} + \sum_{j=1}^{n} N_j A_c H_j\Big|_Z - \sum_{j=1}^{n} N_j A_c H_j\Big|_{Z+dZ} + P_{Per} \times dz \times U \times (T_S - T) - P_{Per} \times dz \times \begin{cases} 0 & j \neq H_2 \\ J_{H_2} \times H_{H_2} & j = H_2, P^t_{H_2} \geq P^s_{H_2} \\ -J_{H_2} \times H^s_{H_2} & j = H_2, P^s_{H_2} \geq P^t_{H_2} \end{cases} = \frac{\partial(\sum_{j=1}^{n} n_j U_j)}{\partial t} \begin{matrix} j = 1,2,...,n \\ i = 1,2,...,m \end{matrix} \quad \text{(A12)}$$

where H_{H_2} and $H^s_{H_2}$ are enthalpy of hydrogen in reaction and permeation sides, respectively. P_{Per} is perimeter of system. U_i is internal energy component j in the system. The Pd-Ag membrane is permeable just for hydrogen and insulated for other components. Therefore, the energy is not transferred by the mass transfer through the membrane layer for other components.

$$-K_{eff}A_c\frac{\partial T}{\partial z}\Big|_Z - K_{eff}A_c\frac{\partial T}{\partial z}\Big|_{Z+dZ} + \sum_{j=1}^{n} N_j A_c H_j\Big|_Z - \sum_{j=1}^{n} N_j A_c H_j\Big|_{Z+dZ} + P_{Per} \times dz \times U \times (T_S - T) - P_{Per} \times dz \times \begin{cases} J_{H_2} \times H_{H_2} & P^t_{H_2} \geq P^s_{H_2} \\ -J_{H_2} \times H^s_{H_2} & P^s_{H_2} \geq P^t_{H_2} \end{cases} = \frac{\partial(\sum_{j=1}^{n} n_j U_j)}{\partial t} \begin{matrix} j = 1,2,...,n \\ i = 1,2,...,m \end{matrix} \quad \text{(A13)}$$

by considering the Taylor's extension one can obtain:

$$\frac{1}{A_c}\frac{\partial}{\partial z}\left(K_{eff}A_c\frac{\partial T}{\partial z}\right)-\frac{1}{A_c}\frac{\partial(\sum_{j=1}^{n}N_jA_cH_j)}{\partial z}+\frac{P_{Per}}{A_c}\times U\times(T_S-T)$$
$$-\frac{P_{Per}}{A_c}\times\begin{cases}J_{H_2}\times H_{H_2} & P^t_{H_2}\geq P^s_{H_2}\\ -J_{H_2}\times H^s_{H_2} & P^s_{H_2}\geq P^t_{H_2}\end{cases}=\frac{1}{A_c.dz}\sum_{j=1}^{n}n_j\frac{\partial U_j}{\partial t}$$
$$+\frac{1}{A_c}\sum_{j=1}^{n}U_j\frac{\partial n_j}{\partial t}\quad(A14)$$

substituting Eqs. A8 and A9 in the above equation, we have:

$$\frac{1}{A_c}\frac{\partial}{\partial z}(K_{eff}A_c\frac{\partial T}{\partial z})-\sum_{j=1}^{n}H_j\frac{\partial N_j}{\partial z}-\sum_{j=1}^{n}N_j\frac{\partial H_j}{\partial z}$$
$$-\frac{1}{A_c}\sum_{j=1}^{n}N_jH_j\frac{\partial A_C}{\partial z}+\frac{P_{Per}}{A_c}\times U\times(T_S-T)$$
$$-\frac{P_{Per}}{A_c}\times\begin{cases}J_{H_2}\times H_{H_2} & P^t_{H_2}\geq P^s_{H_2}\\ -J_{H_2}\times H^s_{H_2} & P^s_{H_2}\geq P^t_{H_2}\end{cases}=\varepsilon\sum_{j=1}^{n}C_j\frac{\partial U_j}{\partial t}$$
$$+\varepsilon\sum_{j=1}^{n}U_j\frac{\partial C_j}{\partial t}\quad(A15)$$

The term $\frac{\partial N_j}{\partial z}$ is not known and is replaced from Eq. A6:

$$\frac{1}{A_c}\frac{\partial}{\partial z}\left(K_{eff}A_c\frac{\partial T}{\partial z}\right)+\sum_{j=1}^{n}H_j\left(\frac{N_j}{A_c}\frac{\partial(A_c)}{\partial z}-a\times\rho_b\sum_{i=1}^{m}v_{ij}r_i\right.$$
$$\left.+\frac{P_{Per}}{A_c}\begin{cases}0 & j\neq H_2\\ J_{H_2} & j=H_2,P^t_{H_2}\geq P^s_{H_2}\\ -J_{H_2} & j=H_2,P^s_{H_2}\geq P^t_{H_2}\end{cases}+\varepsilon\frac{\partial C_j}{\partial t}\right)-\sum_{j=1}^{n}N_j\frac{\partial H_j}{\partial z}$$
$$-\frac{1}{A_c}\sum_{j=1}^{n}N_jH_j\frac{\partial A_c}{\partial z}+\frac{P_{Per}}{A_c}\times U\times(T_S-T)-\frac{P_{Per}}{A_c}$$
$$\times\begin{cases}J_{H_2}\times H_{H_2} & P^t_{H_2}\geq P^s_{H_2}\\ -J_{H_2}\times H^s_{H_2} & P^s_{H_2}\geq P^t_{H_2}\end{cases}=\varepsilon\sum_{j=1}^{m}C_j\frac{\partial U_j}{\partial t}+\varepsilon\sum_{j=1}^{m}U_j\frac{\partial C_j}{\partial t}\quad(A16)$$

thus

$$\frac{1}{A_c}\frac{\partial}{\partial z}\left(K_{eff}A_c\frac{\partial T}{\partial z}\right)+\sum_{j=1}^{n}H_j\left(\frac{N_j}{A_c}\frac{\partial(A_c)}{\partial z}\right)$$
$$-\sum_{j=1}^{n}H_j\left(a\times\rho_b\sum_{i=1}^{m}v_{ij}r_i\right)$$
$$+\sum_{j=1}^{n}\left(H_j\times\frac{P_{Per}}{A_c}\begin{cases}0 & j\neq H_2\\ J_{H_2} & j=H_2,P^t_{H_2}\geq P^s_{H_2}\\ -J_{H_2} & j=H_2,P^s_{H_2}\geq P^t_{H_2}\end{cases}\right)+\sum_{j=1}^{n}H_j\times\varepsilon\frac{\partial C_j}{\partial t}$$
$$-\sum_{j=1}^{n}N_j\frac{\partial H_j}{\partial z}-\frac{1}{A_c}\sum_{j=1}^{m}N_jH_j\frac{\partial A_c}{\partial z}+\frac{P_{Per}}{A_c}\times U\times(T_S-T)-\frac{P_{Per}}{A_c}$$
$$\times\begin{cases}J_{H_2}\times H_{H_2} & P^t_{H_2}\geq P^s_{H_2}\\ -J_{H_2}\times H^s_{H_2} & P^s_{H_2}\geq P^t_{H_2}\end{cases}=\varepsilon\sum_{j=1}^{n}C_j\frac{\partial U_j}{\partial t}+\varepsilon\sum_{j=1}^{n}U_j\frac{\partial C_j}{\partial t}\quad(A17)$$

The second and the seventh terms are canceled.

The fourth term in the above equation can be reduced to:

$$\sum_{j=1}^{n}H_j\left(\frac{P_{Per}}{A_c}\begin{cases}0 & j\neq H_2\\ J_{H_2} & j=H_2,P^t_{H_2}\geq P^s_{H_2}\\ -J_{H_2} & j=H_2,P^s_{H_2}\geq P^t_{H_2}\end{cases}\right)$$
$$=\frac{P_{Per}}{A_c}\sum_{j=1}^{n}\left(\begin{cases}0\times H_j & j\neq H_2\\ J_{H_2}\times H_{H_2} & j=H_2,P^t_{H_2}\geq P^s_{H_2}\\ -J_{H_2}\times H_{H_2} & j=H_2,P^s_{H_2}\geq P^t_{H_2}\end{cases}\right)$$
$$=\frac{P_{Per}}{A_c}\begin{cases}0 & j\neq H_2\\ J_{H_2}\times H_{H_2} & j=H_2,P^t_{H_2}\geq P^s_{H_2}\\ -J_{H_2}\times H_{H_2} & j=H_2,P^s_{H_2}\geq P^t_{H_2}\end{cases}$$
$$=\frac{P_{Per}}{A_c}\begin{cases}J_{H_2}\times H_{H_2}P^t_{H_2}\geq P^s_{H_2}\\ -J_{H_2}\times H_{H_2}P^s_{H_2}\geq P^t_{H_2}\end{cases}\quad(A18)$$

now we have:

$$\frac{1}{A_c}\frac{\partial}{\partial z}\left(K_{eff}A_c\frac{\partial T}{\partial z}\right)-a\times\rho_b\left(\sum_{i=1}^{m}\sum_{j=1}^{n}(H_jv_{ij})r_i\right)-\sum_{j=1}^{n}N_j\frac{\partial H_j}{\partial z}$$
$$+\frac{P_{Per}}{A_c}\times U\times(T_S-T)\frac{P_{Per}}{A_c}\begin{cases}J_{H_2} & P^t_{H_2}\geq P^s_{H_2}\\ -J_{H_2} & P^s_{H_2}\geq P^t_{H_2}\end{cases}-\frac{P_{Per}}{A_c}$$
$$\times\begin{cases}J_{H_2}\times H_{H_2} & P^t_{H_2}\geq P^s_{H_2}\\ -J_{H_2}\times H^s_{H_2} & P^s_{H_2}\geq P^t_{H_2}\end{cases}=\varepsilon\sum_{j=1}^{n}C_j\frac{\partial U_j}{\partial t}+\varepsilon\sum_{j=1}^{n}(U_j-H_j)\frac{\partial C_j}{\partial t}\quad(A19)$$

now the following definitions are used to simplify the recent equation:

$$\Delta H_i=\sum_{j=1}^{n}(H_jv_{ij})\quad(A20)$$

$$\frac{\partial H_j}{\partial z}=\frac{\partial H_j}{\partial T}\times\frac{\partial T}{\partial z}=C_{P_j}\times\frac{\partial T}{\partial z}\quad(A21)$$

$$N_j=J_j+C_ju_Z=-D_{ej}\frac{\partial C_j}{\partial z}+C_ju_Z\quad(A22)$$

$$\sum_{j=1}^{n}N_j\frac{\partial H_j}{\partial z}=\sum_{j=1}^{n}\left((J_j+C_ju_Z)\times C_{P_j}\times\frac{\partial T}{\partial z}\right)$$
$$=\frac{\partial T}{\partial z}\sum_{j=1}^{n}\left((J_j+C_ju_Z)\times C_{P_j}\right)\simeq u_Z\left(\sum_{j=1}^{n}C_jC_{P_j}\right)\frac{\partial T}{\partial z}\quad(A23)$$

$$\left(\sum_{j=1}^{n}C_jC_{P_j}\right)=C_T\left(\sum_{j=1}^{n}\left(\frac{C_j}{C_T}\right)C_{P_j}\right)=C_T\sum_{j=1}^{n}y_jC_{P_j}=C_TC_P\quad(A24)$$

$$(U_j-H_j)=-PV_j=-RT\quad(A25)$$

$$\sum_{j=1}^{n}(U_j-H_j)\frac{\partial C_j}{\partial t}=-RT\sum_{j=1}^{n}\frac{\partial C_j}{\partial t}=-RT\frac{\partial C_T}{\partial t}\quad(A26)$$

$$\frac{\partial U_j}{\partial t} = \frac{\partial U_j}{\partial T} \times \frac{\partial T}{\partial t} = C_{V_j} \times \frac{\partial T}{\partial t} \tag{A27}$$

$$C_{V_j} = C_{P_j} - R \tag{A28}$$

in addition:

$$\sum_{j=1}^{n} C_j \frac{\partial U_j}{\partial t} = \sum_{j=1}^{n} C_j C_{V_j} \times \frac{\partial T}{\partial t} = \frac{\partial T}{\partial t} \sum_{j=1}^{n} C_j C_{V_j} = \frac{\partial T}{\partial t} \sum_{j=1}^{n} C_j C_{V_j} = \left(\sum_{j=1}^{n} C_j C_{V_j} \right) \frac{\partial T}{\partial t} \tag{A29}$$

$$\left(\sum_{j=1}^{n} C_j C_{V_j} \right) = C_T \left(\sum_{j=1}^{n} \left(\frac{C_j}{C_T} \right) C_{V_j} \right) = C_T \sum_{j=1}^{n} y_j C_{V_j} = C_T C_V \tag{A30}$$

where C_V and C_P are the average heat capacities of mixture at constant volume and pressure, respectively. Accordingly, based on the above definition:

$$\frac{1}{A_c} \frac{\partial}{\partial z} \left(K_{eff} A_c \frac{\partial T}{\partial z} \right) - a \times \rho_b \left(\sum_{i=1}^{m} \Delta H_i r_i \right) - \frac{\partial T}{\partial z} \sum_{j=1}^{n} (C_j \times C_{P_j} \times u_Z) + \frac{P_{Per}}{A_c} \times U \times (T_S - T) \frac{P_{Per}}{A_c} \times \begin{cases} J_{H_2} \times (H_{H_2} - H_{H_2} \quad P^t_{H_2} \geq P^s_{H_2} \\ J_{H_2} \times (-H_{H_2} + H^s_{H_2}) \quad P^s_{H_2} \geq P^t_{H_2} \end{cases} = \varepsilon \left(\sum_{j=1}^{n} C_j C_{V_j} \right) \frac{\partial T}{\partial t} - \varepsilon RT \frac{\partial C_T}{\partial t} \tag{A31}$$

and then,

$$\frac{1}{A_c} \frac{\partial}{\partial z} \left(K_{eff} A_c \frac{\partial T}{\partial z} \right) - a \times \rho_b \left(\sum_{i=1}^{m} \Delta H_i r_i \right) - u_Z C_P \frac{\partial T}{\partial z} + \frac{P_{Per}}{A_c} \times U \times (T_S - T) - \frac{P_{Per}}{A_c} \times J_{H_2} \times \left\{ H_{H_2} - \begin{cases} H_{H_2} & P^t_{H_2} \geq P^s_{H_2} \\ H^s_{H_2} & P^s_{H_2} \geq P^t_{H_2} \end{cases} \right\} + \varepsilon RT \frac{\partial C_T}{\partial t} = \varepsilon \times C_T \times C_V \frac{\partial T}{\partial t} \tag{A32}$$

now we define γ_{H_2} and then:

$$\frac{1}{A_c} \frac{\partial}{\partial z} \left(K_{eff} A_c \frac{\partial T}{\partial z} \right) - a \times \rho_b \left(\sum_{i=1}^{m} \Delta H_i r_i \right) - u_Z C_P \frac{\partial T}{\partial z} + \frac{P_{Per}}{A_c} \times U \times (T_S - T) \beta \frac{P_{Per}}{A_c} \times J_{H_2} \times \{ H_{H_2} - \gamma_{H_2} \} + \varepsilon RT \frac{\partial C_T}{\partial t} = \varepsilon \times C_T \times C_V \frac{\partial T}{\partial t} \tag{A33}$$

and in the final analysis γ_{H_2} and β are defined as below[53,56]:

$$\gamma_{H_2} = \left(H^t_{H_2} - H^s_{H_2} \right) U_{HVS} \left(P^t_{H_2} - P^s_{H_2} \right) + H^s_{H_2} = \begin{cases} H^t_{H_2} & P^t_{H_2} \geq P^s_{H_2} \\ H^s_{H_2} & P^t_{H_2} < P^s_{H_2} \end{cases} \tag{A34}$$

$$\beta = U_{HVS} \left(P^t_{H_2} - P^s_{H_2} \right) = \begin{cases} +1 & P^t_{H_2} \geq P^s_{H_2} \\ -1 & P^t_{H_2} < P^s_{H_2} \end{cases} \tag{A35}$$

U_{HVS}: HeavisideFunction

Manuscript received Dec. 22, 2010, and revision received Mar. 13, 2011.